Photoabsorption in Hot Dense Plasmas

W. R. Johnson
Department of Physics – 225 Nieuwland Science Hall
University of Notre Dame
Notre Dame, IN 46556

February 11, 2001

Abstract

This is a preliminary version of the time-dependent local-density approximation designed to study photoabsorption in hot dense plasmas. The theory developed so far is applied to study the photoexcitation in aluminum and helium plasmas and photoionization in aluminum plasmas.

1 Self-consistent LDA at finite temperatures

These notes describe a version of the time-dependent local-density approximation (TDLDA) that can be used to give a multichannel description of photoexcitation and photoionization in a dense plasma. A similar, but less complete, study was carried out earlier by Grimaldi, Grimaldi-Lecourt, and Dharmawardana [1] and used to study light absorption in an iron plasma.

Our point of departure is a muffin-tin local-density approximation (LDA) model for a dense plasma. In this model, an average atom in the plasma is described by a collection of electrons in a neutral, spherically symmetric, potential produced by the nucleus and a thermal distribution of bound and continuum electrons. The electrons are constrained to lie inside a Wigner-Seitz sphere of volume v and radius R determined by the material density ρ_m (g/cm^3) and atomic weight A (g/mol):

$$v = \frac{A}{\mathcal{A}\rho_m}\,, \qquad R = \left(\frac{3v}{4\pi}\right)^{1/3}\,,$$

where $\mathcal{A} = 6.022 \times 10^{23}$ is Avagadro's number. The equations defining our model are solved self-consistently to determine energy levels, level populations, and the self-consistent potential. Our model is similar to, but less complete than, other average atom models, such as INFERNO [2], that have been introduced over the years. The present model is a generalization of the Thomas-Fermi model of a hot dense plasma, introduced a half century ago by Feynman, Metropolis, and Teller [3] and elucidated by Cowan and Ashkin [4].

1.1 Basic Equations

In the model, each bound electron is assumed to satisfy

$$\left[h_0 - \frac{Z}{r} + V\right] u_a(\boldsymbol{r}) = \epsilon_a u_a(\boldsymbol{r})\,, \tag{1.1}$$

where, in the present work, h_0 is taken to be the Dirac Hamiltonian

$$h_0 = c\,\boldsymbol{\alpha}\cdot\boldsymbol{p} + \beta mc^2\,. \tag{1.2}$$

The Dirac equation is used here since it automatically accounts for the fine structure of inner shells.[1] The self-consistent potential $V(r) = V_{\rm dir} + V_{\rm exc}$ which is taken to be a functional of the electron density $\rho(r)$, supports a finite number of bound states. The eigenvalues ϵ_a are approximations to the binding energies of these states. The direct part of the potential is given by

$$V_{\rm dir} = \int d^3x \frac{\rho(x)}{|\boldsymbol{r}-\boldsymbol{x}|}\,, \tag{1.3}$$

where the electron density $\rho = \rho_b + \rho_c$ has contributions from bound and continuum electrons. The bound-electron contribution is

$$\rho_b(r) = \sum_a f_a(T)\,|u_a(\boldsymbol{r})|^2\,, \tag{1.4}$$

where a ranges over all bound states. The factor $f_a(T)$ is the Fermi-Dirac factor

$$f_a(T) = \frac{1}{1+\exp[(\epsilon_a-\mu)/kT]}\,.$$

The contribution from continuum electrons ρ_c is (for the present) evaluated in the semi-classical Thomas-Fermi approximation:

$$\rho_c(r) = \frac{(2mkT)^{3/2}}{2\pi^2}\,I_{1/2}(b,x)\,, \tag{1.5}$$

where $I_j(b,x)$ is the incomplete Fermi-Dirac integral given by

$$I_j(b,x) = \int_b^\infty \frac{y^j\,dy}{1+\exp[y-x]}\,.$$

The arguments of the Fermi-Dirac integral are

$$\begin{aligned} x &= \Big(\mu - V + Z/r\Big)/kT, \quad \text{and} \\ b &= \Big(-V + Z/r\Big)/kT\,. \end{aligned}$$

[1] The Dirac equation was used previously in the plasma studies by Liberman [2], Rozsnyai [5], and Belenski and Ishikawa [6].

A derivation of Eq. (1.5) is given in Appendix A.

The exchange potential is taken to be the Kohn-Sham potential

$$V_{\rm exc} = -\left(\frac{3}{\pi}\,\rho(r)\right)^{1/3} . \tag{1.6}$$

For completeness, we include the derivation of Eq. (1.6) in Appendix B.

Equations (1.1) through (1.6) are solved self consistently. The chemical potential μ is chosen to insure electric neutrality:

$$Z = \int_{r<R} \rho(r)\, d^3r \equiv \int_0^R 4\pi r^2 \rho(r)\, dr\,, \tag{1.7}$$

where R is the muffin-tin radius.

The continuum density is automatically constrained to lie inside the Wigner-Seitz sphere. We impose MIT bag model boundary conditions on the Dirac bound-state wave functions at $r = R$ to insure that $\rho_b(r)$ lies inside the sphere. A short discussion describing how the bag-model boundary conditions are imposed in our point-by-point integration scheme is given in Appendix C.

1.2 Example: Iron at kT=100 eV

As an illustrative example, we solve the above LDA equations for an iron plasma Z=26 and A=55.845 gm/mol at normal density ρ_m=7.874 gm/cc.[2] The corresponding Wigner-Seitz radius is R=2.6672 a_0. In our example, we choose kT=100 eV. In Fig. 1, we show the resulting electron density $\rho(r)$ together with the bound and continuum contributions $\rho_b(r)$ and $\rho_c(r)$. The electron density shown in this figure is indistinguishable from the corresponding result of Rozsnyai given in Fig. 1 of Ref. [5].

It is interesting to compare results from the present model with results from similar models. In Table 1, we compare the binding energies ϵ_{nlj}, the chemical potential μ, the bound-state occupation numbers N_{nlj}, and the number of continuum electrons/ion $N_{\rm cont}$ with nonrelativistic results from [1] and relativistic results from [5] for the plasma considered in Fig. 1. For levels with principal quantum numbers $n \leq 3$, our states are more tightly bound than those of [1] but less tightly bound than those of [5]. Our $4p$ electrons dissolve into the continuum as do those in the [1]. In Ref. [5], the $4p$ levels are bound and there is a second bound $4s$ level, not shown in the table, that was introduced to approximate valance bands in a solid. The chemical potential from the present calculation lies between the values given by the two comparison calculations, as does the number of continuum electrons/ion. At a qualitative level, at least, our average atom model describes the same physics as the comparison models. Our numerical results agree better with the nonrelativistic calculations of [1].

[2]Properties of materials quoted here are taken from the *web-elements* world-wide web site [7].

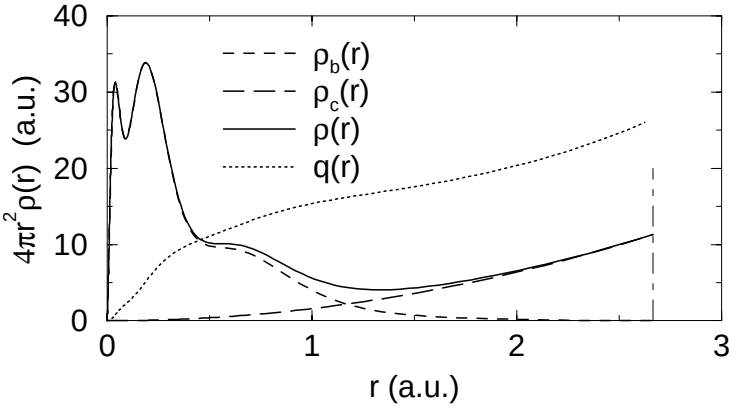

Figure 1: Electron density $4\pi r^2\rho(r)$ of an iron ion in a plasma of normal metallic density and temperature kT=100 eV. Contributions from both bound ρ_b and continuum ρ_c electrons are shown. $q(r)$ is the charge inside a sphere of radius r.

Table 1: Bound-state energies (a.u.) and level populations for an average atom in an iron plasma at normal density and temperature $kT = 100$ eV from the present model are compared with results from other calculations.

	Present		Non. Rel. LDA [1]		Rel. LDA [5]	
Level	ϵ_{nlj}	N_{nlj}	ϵ_{nl}	N_{nl}	ϵ_{nlj}	N_{nlj}
$1s$	-261.251	2.0000	-258.140	2.0000	-266.021	2.0000
$2s$	-34.205	1.9988	-32.942	1.9984	-35.746	1.9990
$2p_{1/2}$	-30.186	1.9964	-29.008	1.9954	-31.831	1.9972
$2p_{3/2}$	-29.721	3.9919	-29.008	3.9908	-31.363	3.9937
$3s$	-6.246	0.9087	-5.411	0.8234	-6.524	0.8506
$3p_{1/2}$	-5.005	0.7453	-4.195	0.6690	-5.283	0.6912
$3p_{3/2}$	-4.926	1.4707	-4.195	1.3380	-5.196	1.3611
$3d_{3/2}$	-2.945	1.0131	-2.218	0.9076	-3.233	0.9286
$3d_{5/2}$	-2.933	1.5159	-2.218	1.3614	-3.218	1.3886
$4s$	-0.351	0.2868	-0.166	0.2876	-0.533	0.9709
$4p_{1/2}$					-0.186	0.0442
$4p_{3/2}$					-0.174	0.0881
$N_{\rm bound}$		15.9277		15.3716		16.4547
$N_{\rm cont}$		10.0723		10.6284		9.5453
μ (a.u.)		-6.9187		-6.7232		-7.6302

2 Time-Dependent LDA Equations

In this section, we set up the version of the TDLDA that we use to investigate photoabsorption in a dense plasma. To this end, we consider the response of an average atom in the plasma to an applied time-dependent perturbation. We will later associate the perturbation with an incident photon beam and use the equations developed here to study photoabsorption in the plasma. The nonrelativistic TDLDA was developed and used to study photoionization of free atoms by Zangwill and Soven [8], and, as mentioned earlier, a nonrelativistic version of the TDLDA was used in Ref. [1] to study photoionization in hot dense plasmas. A relativistic version of the TDLDA for free atoms was developed by Parpia [9] and applied to study atomic photoionization [10, 11] and polarizabilities [12] of atoms. In the paragraphs below, we set up a version of the relativistic TDLDA appropriate to our plasma model. The TDLDA is closely related to the random-phase approximation (RPA). In fact, if we were to apply the arguments below to an atom in a Dirac-Hartree-Fock (DHF) ground state, then we obtain would the equations of the relativistic RPA, as shown in Ref. [13]. The TDLDA can be considered as a simplified version of the RPA. Both the TDLDA and the RPA account for interchannel coupling. The RPA also accounts for the modified potential seen by the ionized electron, whereas a the TDLDA does not. Formalism for the RPA in a plasma has been given by des Cloizeaux [14] and by Csanak and Kilcrease [15], and a single channel version of the RPA has been used to study a He atom in a dense plasma by Csanak and Meneses in Ref. [16].

2.1 Basic Inhomogeneous Equations

Let us introduce a time-dependent interaction

$$V_{\rm int}(\boldsymbol{r},t) = -e\left[\phi(\boldsymbol{r})e^{-i\omega t} + \phi^{\dagger}(\boldsymbol{r})e^{i\omega t}\right] \tag{2.1}$$

into a plasma described in the average atom LDA. The result is that the single-particle orbitals become time dependent;

$$u_a(\boldsymbol{r}) \rightarrow \psi_a(\boldsymbol{r},t).$$

These time-dependent orbitals satisfy the time-dependent generalization of the plasma orbital equations

$$-i\frac{\partial\psi_a}{\partial t} = \left[h_0 - \frac{Z}{r} + V(\rho,\boldsymbol{r}) + V_{\rm int}(\boldsymbol{r},t)\right]\psi_a. \tag{2.2}$$

In this equation,

$$\rho(\boldsymbol{r},t) = \sum_b f_b(T)\ \psi_b^{\dagger}(\boldsymbol{r},t)\,\psi_b(\boldsymbol{r},t) + \rho_{\rm c}(\boldsymbol{r},t)\,. \tag{2.3}$$

The function $f_b(T)$ is the Fermi-Dirac weight factor for state b determined from a time-independent average atom calculation. The quantity $\rho_c(\boldsymbol{r},t)$ is the contribution to the density from continuum electrons. In the present model, we treat the continuum in a semi-classical approximation and ignore the time dependence of ρ_c.

We assume that the time-dependent orbital wave function $\psi_a(\boldsymbol{r}.t)$ has the form

$$\psi_a(\boldsymbol{r},t) = \left[u_a(\boldsymbol{r}) + w_{a+}(\boldsymbol{r})\, e^{-i\omega t} + w_{a-}(\boldsymbol{r})\, e^{i\omega t}\right] e^{-i\epsilon_a t}\ . \tag{2.4}$$

Substituting this wave function into Eq. (2.2), linearizing the right-hand side in powers of the perturbing potential, and identifying terms with the same time dependence on the right and left hand sides, we obtain

$$\left[h_0 - \frac{Z}{r} + V(\rho_0,\boldsymbol{r})\right] u_a(\boldsymbol{r}) = \epsilon_a\, u_a(\boldsymbol{r}) \tag{2.5}$$

for the lowest-order terms, where

$$\rho_0(\boldsymbol{r}) = \sum_b f_b(T)\ |u_b(\boldsymbol{r})|^2 + \rho_{\rm c}(\boldsymbol{r})\,. \tag{2.6}$$

Eq. (2.5), which is identical to Eq. (1.1), describes bound-states in the unperturbed average atom. The first-order perturbations $w_{a\pm}(\boldsymbol{r})$ satisfy

$$\left[h_0 - \frac{Z}{r} + V(\rho_0) - (\epsilon_a + \omega)\right] w_{a\,+}(\boldsymbol{r}) + \delta V_+\, u_a(\boldsymbol{r}) = e\phi(\boldsymbol{r})\, u_a(\boldsymbol{r}) \tag{2.7}$$

$$\left[h_0 - \frac{Z}{r} + V(\rho_0) - (\epsilon_a - \omega)\right] w_{a\,-}(\boldsymbol{r}) + \delta V_-\, u_a(\boldsymbol{r}) = e\phi^\dagger(\boldsymbol{r})\, u_a(\boldsymbol{r}), \tag{2.8}$$

where $\delta V_\pm$ are the positive and negative components of the perturbed potential. In the present model, the perturbed potential is given by

$$\delta V_\pm = \delta V_{{\rm dir}\,\pm} + \delta V_{{\rm exc}\,\pm}.$$

From Eq. (1.3), it follows that the perturbed direct potential is

$$\delta V_{{\rm dir}\,\pm} \equiv \int d^3x \frac{\rho_\pm(\boldsymbol{x})}{|\boldsymbol{r}-\boldsymbol{x}|}\,, \tag{2.9}$$

where the perturbed density is

$$\rho_\pm(\boldsymbol{r}) = \sum_b f_b(T)\left[w^\dagger_{b\mp}(\boldsymbol{r})\, u_b(\boldsymbol{r}) + u^\dagger_b(\boldsymbol{r})\, w_{b\pm}(\boldsymbol{r})\right]. \tag{2.10}$$

The perturbed exchange potential is

$$\delta V_{{\rm exc}\,\pm} = -\frac{1}{3}\left(\frac{3}{\pi}\,\rho_0\right)^{1/3} \frac{\rho_\pm}{\rho_0}\,. \tag{2.11}$$

Putting the direct and exchange parts together, we find that the perturbed potential contribution to Eqs. (2.7) and (2.8) is

$$\delta V_\pm = \int d^3x \frac{\rho_\pm(\boldsymbol{x})}{|\boldsymbol{r}-\boldsymbol{x}|} - \frac{1}{3}\left(\frac{3}{\pi}\,\rho_0\right)^{1/3} \frac{\rho_\pm}{\rho_0}\,. \tag{2.12}$$

2.2 Homogeneous TDLDA

It is of interest to study the homogeneous equations obtained by setting the right-hand sides of Eqs. (2.7) and (2.8) to zero:

$$\left[h_0 - \frac{Z}{r} + V(\rho_0) - \epsilon_a\right] w_{a\,+}(\boldsymbol{r}) + \delta V_+\, u_a(\boldsymbol{r}) = \omega\, w_{a\,+}(\boldsymbol{r}) \tag{2.13}$$

$$\left[h_0 - \frac{Z}{r} + V(\rho_0) - \epsilon_a\right] w_{a\,-}(\boldsymbol{r}) + \delta V_-\, u_a(\boldsymbol{r}) = -\omega\, w_{a\,-}(\boldsymbol{r})\,. \tag{2.14}$$

These coupled equations constitute a linear eigenvalue problem for the excitation energy ω. If we let $w^{\lambda}_{a\pm}(\boldsymbol{r})$ be the the set of perturbed eigenfunctions belonging to the eigenvalue ω_λ, then we obtain the following orthogonality relation:

$$\sum_a \int d^3r \left[w^{\lambda\dagger}_{a\,+}(\boldsymbol{r}) w^{\mu}_{a\,+}(\boldsymbol{r}) - w^{\mu\dagger}_{a\,-}(\boldsymbol{r}) w^{\lambda}_{a\,-}(\boldsymbol{r})\right] = \mathrm{sign}(\omega_\lambda)\,\delta_{\lambda\mu} \tag{2.15}$$

Expanding the solutions to the inhomogeneous Eqs. (2.7) and (2.8) in terms of the eigenfunctions of the homogeneous Eqs. (2.13) and (2.14), we find

$$w_{a\,+}(\boldsymbol{r}) \;=\; \sum_\mu \frac{T_\mu}{\omega - \omega_\mu}\, w^{\mu}_{a\,+}(\boldsymbol{r}) \tag{2.16}$$

$$w^{\dagger}_{a\,-}(\boldsymbol{r}) \;=\; \sum_\mu \frac{T_\mu}{\omega - \omega_\mu}\, w^{\mu\dagger}_{a\,-}(\boldsymbol{r})\,, \tag{2.17}$$

where

$$T_\mu = -e \sum_a \int d^3r \left[w^{\mu\dagger}_{a\,+}(\boldsymbol{r})\phi(\boldsymbol{r})u_a(\boldsymbol{r}) + u^{\dagger}_a(\boldsymbol{r})\phi(\boldsymbol{r}) w^{\mu}_{a\,-}(\boldsymbol{r})\right]\,. \tag{2.18}$$

The time-dependent atomic wave function, therefore, has poles at the eigenvalues ω_μ with residues T_μ. Comparing with perturbation theory, one concludes that the (positive) frequencies ω_μ are excitation energies of the atom and that T_μ is the amplitude of the transition from the unperturbed state, which is described by orbitals $u_a(\boldsymbol{r})$, to the μ-th excited state of the atom.

2.3 Angular Decomposition

In this section we carry out the angular momentum decomposition of the homogeneous TDLDA functions $w_{a\,\pm}$ introduced in the previous section. We choose the solutions to the homogeneous equations in such a way that they describe a perturbed state of the average atom that has angular momentum (JM). To understand just how such solutions are constructed, we first note that in the time-dependent picture the unperturbed many electron wave function is a Slater determinant that oscillates with frequency $E_0 = \sum_a \epsilon_a$. The part of the

perturbed many-electron wave function that oscillates with frequency $E_0 + \omega$ consists of a sum of Slater determinants in which each orbital u_a is replaced by its associated perturbed orbital w_{a+}. The many-electron wave function produced by removing orbital $a : (j_a, m_a)$ has angular momentum $(j_a, -m_a)$. Replacing u_a by an excited orbital w_{a+} with angular momentum (j_m, m_m) leads to an excited state that has indefinite angular momentum; however, replacing u_a with the coupled "particle-hole" linear combination of excited orbitals, described below, leads to an excited state with angular momentum (JM).

2.3.1 Radial TDLDA Equations

To construct a many-electron wave function describing the excitation of the spherically symmetric ($J = 0$, $M = 0$) average atom to a state with angular momentum $(J\,M)$, we expand the perturbation $w_{a\pm}$ as a linear combination of Dirac angular momentum states $w^{JM}_{am\pm}(\boldsymbol{r})$:

$$w_{a+}(\boldsymbol{r}) = \sum_m (-1)^{j_a - m_a} \langle j_a - m_a, j_m\, m_m | JM \rangle\, w^{JM}_{am+}(\boldsymbol{r}) \tag{2.19}$$

$$w_{a-}(\boldsymbol{r}) = \sum_m (-1)^{j_a - m_a + M} \langle j_a - m_a, j_m\, m_m | J - M \rangle\, w^{JM}_{am-}(\boldsymbol{r})\,. \tag{2.20}$$

The coupling coefficients are those appropriate to a particle-hole excitation of a closed-shell system. With this expansion, the perturbed many-body wave function has angular momentum $(J\,M)$.

The perturbed orbitals $w^{JM}_{am\pm}(\boldsymbol{r})$ describe individual excitation channels $a \to m$ contributing to the excited state. These orbitals can be decomposed into radial and angular parts in the usual way:

$$w^{JM}_{am\pm}(\boldsymbol{r}) = \frac{1}{r} \begin{pmatrix} i\,S^J_{am\pm}(r) & \Omega_{\kappa_m m_m}(\hat{r}) \\ T^J_{am\pm}(r) & \Omega_{-\kappa_m m_m}(\hat{r}) \end{pmatrix}. \tag{2.21}$$

We designate the two-component radial function associated with $w^{JM}_{am\pm}$ by

$$R^J_{am\pm}(r) = \begin{pmatrix} S^J_{am\pm}(r) \\ T^J_{am\pm}(r) \end{pmatrix}. \tag{2.22}$$

Similarly, the unperturbed orbital $u_a(\boldsymbol{r})$ is given by

$$u_a(\boldsymbol{r}) = \frac{1}{r} \begin{pmatrix} i\,G_a(r) & \Omega_{\kappa_a m_a}(\hat{r}) \\ F_a(r) & \Omega_{-\kappa_a m_a}(\hat{r}) \end{pmatrix}, \tag{2.23}$$

and the two-component radial orbital corresponding to $u_a(\boldsymbol{r})$ is given by

$$F_a(r) = \begin{pmatrix} P_a(r) \\ Q_a(r) \end{pmatrix}. \tag{2.24}$$

Using the above expansion, we can rewrite the radial density ρ_+ from Eq. (2.10) in terms of the radial orbitals as

$$\rho_+(\boldsymbol{r}) = (-1)^{J-1}\sqrt{4\pi}\, Y_{JM}(\hat{r})\times \\ \frac{1}{4\pi r^2}\sum_{bn} f_b(T)\langle b||C_J||n\rangle \left[R^{J\dagger}_{bn\,-}(r)F_b(r) + F^\dagger_b(r)R^J_{bn\,+}(r)\right] . \quad (2.25)$$

With the aid of these equations, one finds

$$\delta V_{\mathrm{dir}\,+} = (-1)^{J-1}\sqrt{4\pi}\; Y_{JM}(\hat{r})\; \sum_{bn} f_b(T)\frac{\langle b||C_J||n\rangle}{[J]} v_J([nb],r)\,, \quad (2.26)$$

where

$$v_J([nb],r) = \int_0^\infty \frac{r^J_<}{r^{J+1}_>}\; \left[R^{J\dagger}_{bn-}(r)\, F_b(r) + F^\dagger_b(r)R^J_{bn+}(r)\right]\, dr. \quad (2.27)$$

Similarly,

$$\delta V_{\mathrm{exc}\,+} = (-1)^{J-1}\sqrt{4\pi}\; Y_{JM}(\hat{r})\;\; \left.\frac{\partial V_{\mathrm{exc}}}{\partial\rho}\right|_0 \times \\ \frac{1}{4\pi r^2}\sum_{bn} f_b(T)\,\langle b||C_J||n\rangle \left[R^{J\dagger}_{bn-}(r)\, F_b(r) + F^\dagger_b(r)R^J_{bn+}(r)\right], \quad (2.28)$$

where

$$\left.\frac{\partial V_{\mathrm{exc}}}{\partial\rho}\right|_0 \equiv \frac{1}{3\rho_0}V_{\mathrm{exc}}(\rho_0) \equiv -\frac{1}{3\rho_0}\left(\frac{3}{\pi}\rho_0\right)^{1/3} . \quad (2.29)$$

Now, we note that

$$(-1)^{J-1}\sqrt{4\pi}\; Y_{JM}(\hat{r})\, u_a(\boldsymbol{r}) = \sum_{\kappa_m m_m} (-1)^{j_a-m_a}\langle j_a - m_a, j_m\, m_m|JM\rangle \times \\ \langle a||C_J||m\rangle\; \frac{1}{r}\begin{pmatrix} i\,P_a(r) & \Omega_{\kappa_m m_m}(\hat{r}) \\ Q_a(r) & \Omega_{-\kappa_m m_m}(\hat{r})\end{pmatrix}.$$

Combining the above equations, we can rewrite Eq. (2.13) as a radial Dirac equation

$$\left[H_0(\kappa_m) - \frac{Z}{r} + V(\rho_0)\right] R^J_{am\,+}(r) + \langle a||C_J||m\rangle\, \delta V(r)\, F_a(r) \\ = (\epsilon_a + \omega)R^J_{am\,+}(r), \quad (2.30)$$

where the perturbed radial potential is

$$\delta V(r) = \sum_{bn} f_b(T)\frac{\langle b||C_J||n\rangle}{[J]} v_J([nb],r) + \left.\frac{\partial V_{\mathrm{exc}}}{\partial\rho}\right|_0 \times \\ \frac{1}{4\pi r^2}\sum_{bn} f_b(T)\,\langle b||C_J||n\rangle \left[R^{J\dagger}_{bn-}(r)\, F_b(r) + F^\dagger_b(r)R^J_{bn+}(r)\right]. \quad (2.31)$$

and where the unperturbed potential $V(\rho_0)$ is given in Sec. 1. In a similar way, it follows that

$$\left[H_0(\kappa_m) - \frac{Z}{r} + V(\rho_0)\right] R^J_{am\,-}(r) + \langle a||C_J||m\rangle\, \delta V(r)\, F_a(r) = (\epsilon_a - \omega) R^J_{am\,-}(r). \quad (2.32)$$

Equations (2.30), (2.31), and (2.32) are the basic equations of the TDLDA. It should be noticed that the perturbed potential δV couples all excitation channels; it also couples positive and negative frequency excitations. Indeed, when we ignore δV, the positive frequency radial orbital $R^J_{bn+}(r)$ satisfies the radial Dirac equation for an electron with energy $\epsilon_a + \omega$ in the unperturbed potential $V(\rho_0)$ that can be used to study photoionization in the independent-particle approximation (IPA):

$$\left[H_0(\kappa_m) - \frac{Z}{r} + V(\rho_0)\right] R_{am}(r) = (\epsilon_a + \omega) R_{am}(r). \quad (2.33)$$

2.3.2 Multipole Transition Amplitude

Let us replace the perturbing potential in Eq. (2.18) by a multipole potential

$$e\phi(\boldsymbol{r}) \to \phi_{kq}(\boldsymbol{r}) = C_{kq}(\hat{r})\, \phi_k(r), \quad (2.34)$$

where

$$C_{kq}(\hat{r}) = \sqrt{\frac{2k+1}{4\pi}}\, Y_{kq}(\hat{r}).$$

The transition amplitude from the ground state to the excited state (JM) studied in the previous subsection is given by Eq. (2.18), which can be rewritten

$$T_\mu \to \langle JM|T_{kq}|00\rangle = \sum_{am} \Bigg[(-1)^{j_a - m_a} \langle j_a - m_a, j_m\, m_m | JM\rangle \int d^3r\, w^{J\dagger}_{am+}(\boldsymbol{r}) \phi_{kq}(\boldsymbol{r}) u_a(\boldsymbol{r}) + (-1)^{j_a - m_a + M} \langle j_a - m_a, j_m\, m_m | J - M\rangle \int d^3r\, u^\dagger_a(\boldsymbol{r}) \phi_{kq}(\boldsymbol{r}) w^J_{am-}(\boldsymbol{r})\Bigg]. \quad (2.35)$$

Carrying out the sum over magnetic substates, the reduced matrix element of T (which vanishes unless $k = J$) can be written in terms of radial functions only as

$$\langle J||T_k||0\rangle = \delta_{Jk}(-1)^{J-1} \times \sum_{am} \langle a||C_J||m\rangle \int_0^\infty dr\, \left[R^J_{am+}(r)\phi_J(r)F_a(r) + F_a(r)\phi_J(r)R^J_{am-}(r)\right]. \quad (2.36)$$

2.4 Photoexcitation and Photoionization

Photoexcitation rates and photoionization cross sections in the average-atom model of a plasma can be evaluate following the well-known methods used in free atoms. We treat these processes in the dipole approximation and use Eq. (2.36) to evaluate reduced dipole matrix elements. Since the average atom is spherically symmetric, dipole excitations always lead to states with J=1 in this model. We begin by recalling a few basic formulas for photoexcitation.

Photoexcitation The Einstein A-coefficient, giving the probability per unit time for a transition from the average atom state $|a\rangle$ to an excited state $|m\rangle$ with J_m=1 is

$$A_{ma} = \frac{4}{3}\frac{\omega^3}{c^2} S_{ma}, \tag{2.37}$$

where the line strength $S_{ma} = |\langle m\|T_1\|a\rangle|^2$, ω is the excitation energy, and c is the speed of light. We can express A_{ma}, alternatively, as

$$A_{ma} = \frac{16\pi}{3} k^3 S_{ma}\ (R_y c) = \frac{2.02613\times 10^{18}}{\lambda^3}\ S_{ma}\ (\mathrm{s}^{-1}). \tag{2.38}$$

Here, R_y is the Rydberg constant and λ is expressed in (Å). The dimensionless (absorption) oscillator strengths f_{ma} for transitions from the ground state $|a\rangle$ to an excited state $|m\rangle$ is defined in terms of the line strength S_{ma} by the relation

$$f_{ma} = \frac{2}{3}\omega S_{ma} = \frac{303.756}{\lambda} S_{ma}, \tag{2.39}$$

where, again, λ is expressed in (Å).

Photoionization A detailed description of the theory of photoionization in the nonrelativistic RPA was given by Amusia and Cherepkov a quarter century ago in Ref. [17] and a similar, but less exhaustive, description of photoionization in the relativistic RPA was given two decades ago in Refs. [18] and [19]. The formalism developed in [18, 19] can be used without alteration in our relativistic TDLDA study of plasmas. Indeed, this formalism was previously used in Refs. [10] and [11] to carry out relativistic TDLDA calculations of photoionization cross sections and angular distributions in free atoms.

The differential cross section for photoionizing a closed-shell system leaving a ion with a vacancy in subshell a can be written

$$\frac{d\sigma_a}{d\Omega} = \frac{\sigma_a}{4\pi}\Big[1 + \beta_a P_2(\cos\theta)\Big], \tag{2.40}$$

where σ_a is the integrated cross section and β_a is the angular-distribution asymmetry parameter. The angle θ in the above equation is the angle between the outgoing photoelectron momentum vector $\boldsymbol{p}$ and the photon polarization vector $\boldsymbol{\varepsilon}$, as illustrated in Fig. 2. The quantities σ_a and β_a can be evaluated in terms of the reduced dipole matrix element as shown below.

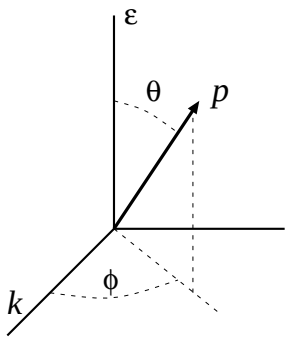

Figure 2: Coordinate system used for the photoelectron angular distribution.

To describe the photoionization process discussed above, we consider final states in which an orbital u_a in subshell (n_a, κ_a) is excited to a perturbed orbital w^1_{am+} with (ϵ_m, κ_m) in the continuum by a photon with energy $\omega = \epsilon_m - \epsilon_a$. The resulting final state is referred to as an excitation channel. Each subshell (n_a, κ_a) is associated with three possible energy degenerate excitation channels satisfying dipole selection rules[3] $\kappa_m = -\kappa_a, \kappa_a \pm 1$. All three channels contribute to the cross section σ_a. For a given value of ω, other channels in which a bound electron (n_b, κ_b) is excited to (ϵ_n, κ_n), with $\epsilon_n = \epsilon_b + \omega$, are energy degenerate with the original three channels. These channels are, in principal, distinguishable from the first three, since they lead to continuum electrons with energies ϵ_n different from ϵ_m. However, all possible energy degenerate channels contribute to the photoabsorption cross section. In the RPA and TDLDA, all possible energy degenerate channels are also included coherently in the sum over $(b\,m)$ in the expression for the reduced matrix element given in Eq. (2.36). The rather complicated analysis of photoionization in the multichannel case is given in detail in Ref. [18]. Below, we outline the simpler analysis in the independent-particle approximation.

Independent Particle Approximation Let us consider the IPA obtained from the TDLDA by neglecting δV. In the IPA, the radial equations (2.33) govern the continuum orbital w^1_{am+}. We choose solutions to orbital equations (2.33) that are regular at the origin and normalized on the energy scale. The resulting phase shifts δ_m depend on the orbital energy ϵ_m. We ignore all other excitation channels (nb) and the negative-frequency excitations R^1_{am-}. We then find that the reduced dipole matrix element in Eq. (2.36) takes the form $\langle m \| T_1 \| a \rangle \rightarrow (-1)^{j_m - j_a} D_{ma}$, where D_{na} is the reduced dipole matrix

[3] If $\kappa_a = -1$, only $\kappa_m = 1$ or $\kappa_m = -2$ are possible; similarly, if $\kappa_a = 1$, only $\kappa_m = -1$ and $\kappa_m = 2$ are possible.

element between single-particle orbitals only:

$$D_{ma} = \langle w^1_{am+} \| \phi_1 \| u_a \rangle = \langle m \| C_1 \| a \rangle \int_0^\infty dr R^1_{am+}(r)\, r\, F_a(r)\,. \tag{2.41}$$

It is convenient to introduce the complex dipole matrix element

$$\mathcal{D}_{am} = i^{-l_m+1} e^{i\delta_m} D_{ma}\ . \tag{2.42}$$

The cross section for ionization of subshell a can then be written

$$\sigma_a = \frac{4\pi^2\alpha}{3}\,\omega \sum_m |\mathcal{D}_{ma}|^2\ , \tag{2.43}$$

where the sum is over the three channels having $\kappa_m = -\kappa_a, \kappa_a \pm 1$. Since the final-state orbitals are normalized on the energy scale, we may write the differential oscillator strength, following Eq. (2.39), in the form

$$\frac{df_{ma}}{dE} = \frac{2}{3}\,\omega\,|\mathcal{D}_{ma}|^2\,. \tag{2.44}$$

From this, it follows that the cross section can be expressed in atomic units as

$$\sigma_a = 2\pi^2\alpha \sum_m \frac{df_{ma}}{dE} \quad (a_0^2). \tag{2.45}$$

Transforming to the more usual megabarn (Mb) units, we find

$$\sigma_a = 4.0336 \sum_m \frac{df_{ma}}{dE} \quad \text{(Mb)}. \tag{2.46}$$

For the record, we note that the angular distribution asymmetry parameter for photoelectrons from subshell a is given by

$$\beta_a = \frac{1}{\bar\sigma_a} \sum_{\kappa_m \kappa_{m'}} \sqrt{30}\,\langle \kappa_{m'} || C_2 || \kappa_m \rangle\,(-1)^{j_{m'}+j_a} \left\{ \begin{array}{ccc} 1 & 1 & 2 \\ j_{m'} & j_m & j_a \end{array} \right\} \Re[\mathcal{D}_{am}\mathcal{D}^*_{am'}]\,, \tag{2.47}$$

where

$$\bar\sigma_a = \sum_m |\mathcal{D}_{ma}|^2\ .$$

2.5 Applications: Discrete Transitions

Aluminum A study of the temperature and density dependence of photoabsorption in an average-atom model was published a quarter century ago by Rozsnyai [20] and applied to aluminum and cesium. Although photoionization cross sections were given for various temperatures, oscillator strengths for discrete transitions were given only for $kT = 0$. It is of interest to reconsider the

Table 2: Orbital energies ϵ_{nlj} and occupation numbers N_{nlj} for a average atom in an Al (Z=13) plasma with density ρ_m=0.027 gm/cc (0.01 $\times$ metallic density) at temperature kT=10eV. The chemical potential is $\mu = -1.801$ and the Wigner-Seitz radius is R=13.879 a_0.

Shell	ϵ_{nlj}	N_{nlj}	Shell	ϵ_{nlj}	N_{nlj}
$1s_{1/2}$	-56.10808	2.0000	$4s_{1/2}$	-0.19808	0.0252
$2s_{1/2}$	-4.73745	1.9993	$4p_{1/2}$	-0.12799	0.0209
$2p_{1/2}$	-3.36223	1.9718	$4p_{3/2}$	-0.12762	0.0417
$2p_{3/2}$	-3.34575	3.9411	$4d_{3/2}$	-0.04027	0.0329
$3s_{1/2}$	-0.78759	0.1193	$4d_{5/2}$	-0.04023	0.0494
$3p_{1/2}$	-0.53671	0.0621	$5s_{1/2}$	-0.02667	0.0159
$3p_{3/2}$	-0.53526	0.1238	$4f_{5/2}$	-0.01606	0.0463
$3d_{3/2}$	-0.23642	0.0559	$4f_{7/2}$	-0.01604	0.0617
$3d_{5/2}$	-0.23638	0.0838			
			$N_{\rm bound}$		10.6511
			$N_{\rm cont.}$		2.3489

discrete transitions in this case for finite temperatures. Our average-atom code gave the results shown in Table 2 for energies and occupation numbers in an Al plasma at density 0.027 gm/cc and temperature kT=10eV. As seen from the table, the 10 electron Ne-like core is almost completely occupied and 2.3 of the remaining 3 electrons are in the continuum. The bound n=3, 4, and 5 levels are sparsely occupied at kT=10 eV.

There are 54 allowed electric-dipole transitions between the average-atom levels shown in Table 2. We give the transition energies ΔE and absorption oscillator strengths f_{jj} for strongest of these transitions ($2s \rightarrow 3p$, $2p \rightarrow 3s$, and $2p \rightarrow 3d$) in columns 2 and 3, respectively, of Table 3. Sums over j values belonging to a given l are carried out to give the oscillator strengths f_L in column 5. It is instructive to compare the model energies and oscillator strengths with corresponding values for Ne-like ion Al^{+3}. The present energies are about 10% smaller than energies $\Delta E_{\rm ion}$ for the free ion given in column 4 of Table 3. The oscillator strengths f_L, on the other hand, are smaller than the free-ion values $f_{\rm ion}$, given in column 6 of the table, by a factor of 2. In this regard, it should be mentioned that correlation corrections are known to be very important in low-Z ions such as Al^{+3}. Indeed, the *uncorrelated* Al^{+3} oscillator strengths $f^{(0)}_{\rm ion}$ given in the 7th column of Table 3 are in closer agreement with the present values. This example points up the necessity of including correlation effects in average-atom calculations. The dominant correlation corrections to oscillator strengths will be, as a matter of fact, included in the coupled TDLDA

Table 3: Excitation energies ΔE and absorption oscillator strengths f_{jj} for transitions between average-atom levels in an Al plasma of density ρ_m=0.027 gm/cc and temperature kT=10 eV calculated in the IPA. The quantities f_L are sums of oscillator strengths for levels with same initial and final l values. Comparison values for the energies $\Delta E_{\rm ion}$ and oscillator strengths $f_{\rm ion}$ for the ion Al^{+3} are from relativistic MBPT calculations [21]. Uncorrelated oscillator strengths $f^{(0)}_{\rm ion}$ for Al^{+3} are from DHF calculations.

Transition	ΔE	f_{jj}	$\Delta E_{\rm ion}$	f_L	$f_{\rm ion}$	$f^{(0)}_{\rm ion}$
$2s_{1/2} \rightarrow 3p_{1/2}$	4.201	0.03481				
$2s_{1/2} \rightarrow 3p_{3/2}$	4.202	0.06797	4.927	0.1028	0.1891	0.0614
$2p_{1/2} \rightarrow 3s_{1/2}$	2.575	0.04889				
$2p_{3/2} \rightarrow 3s_{1/2}$	2.558	0.09948	2.796	0.1484	0.2828	0.1592
$2p_{1/2} \rightarrow 3d_{3/2}$	3.126	0.16092				
$2p_{3/2} \rightarrow 3d_{3/2}$	3.109	0.03249				
$2p_{3/2} \rightarrow 3d_{5/2}$	3.109	0.29236	3.455	0.4858	0.9714	0.4000

calculations.

Helium Csanak and Meneses recently developed a temperature-dependent single-channel version of the RPA, referred to as the SCRPA and applied it to helium at low temperatures. This calculation automatically includes the dominant correlation corrections discussed in the previous section. As mentioned earlier, the SCRPA is closely related to the TDLDA. In Table 4, we compare average-atom energy levels and occupation numbers for a several states in He at density 1.5×10^{19} atoms/cc and temperature kT=10 eV obtained from the present LDA code with values from Rozsnayi [22], and with values from the INFERNO code [2] used as input in the SCRPA calculation. Except for the occupation numbers from [22] shown in column 5, which are conjectured to be misprints, the three calculations are in fair agreement. In Table 5, we compare transition energies and oscillator strengths from the present calculation in He at density 1.5×10^{19} atoms/cc and temperature kT=10 eV with values from the calculations of [22] and with SCRPA calculations [16]. The values of f_L from [22] were multiplied by 0.1630 to give the values shown in parentheses in column 5 of the table. This factor corresponds to an omitted initial state occupation factor in the oscillator strengths given in [22], which are remarkably close to values for the free He^{+1} ion. Assuming that the initial state occupation number $N_{1s} = 0.0630$ given in Ref. [22], was a misprint of $N_{1s} = 0.1630$, and that this value was omitted in the calculations of f_L, we obtain the values shown in parentheses in Table 5. These conjectures have yet to be confirmed with Dr.

Table 4: Average-atom energy levels ϵ_{nl} and occupation numbers N_{nl} for a few states in He (Z=2) at density 1.5×10^{19} atoms/cc and temperature kT=10 eV are compared with values from other calculations.

	Present		Rozsnyai [22]		INFERNO [2]	
Shell	ϵ_{nl}	N_{nl}	ϵ_{nl}	N_{nl}	ϵ_{nl}	N_{nl}
$1s$	-2.0474	0.1330	-2.0000	0.0630	-2.1901	0.1707
$2p$	-0.4240	0.0051	-0.4427	0.0028	-0.4429	0.0048
$3p$	-0.1516	0.0024	-0.1670	0.0013	-0.1611	0.0022
$4p$	-0.0624	0.0020	-0.0729	0.0010	-0.0709	0.0017
$5p$	-0.0255	0.0018	-0.0317	0.0009	-0.0346	0.0016
$6p$	-0.0038	0.0016	-0.0132	0.0009		
$N_{\rm bound}$		0.1854		0.100?		0.2060
μ	-3.0184				-3.0618	

Table 5: Transition energies ΔE and oscillator strengths f_L from the present calculation in He at density 1.5×10^{19} atoms/cc and temperature kT=10 eV are compared with values from the calculations of [22] (modified as described in the text) and with the SCRPA calculations of [16].

	Present		Rozsnyai [22]		SCRPA [16]	
Transition	ΔE	f_L	ΔE	f_L	ΔE	f_L
$1s \rightarrow 2p$	1.6234	0.05433	1.5574	(0.05700)	1.7093	0.07203
$1s \rightarrow 3p$	1.8958	0.00978	1.8331	(0.01221)	2.0117	0.01221
$1s \rightarrow 4p$	1.9851	0.00337	1.9272	(0.00443)	2.1096	0.00418
$1s \rightarrow 5p$	2.0219	0.00140	1.9684	(0.00195)	2.1500	0.00164
$1s \rightarrow 6p$	2.0436	0.00136	1.9869	(0.00085)	2.1607	0.00003

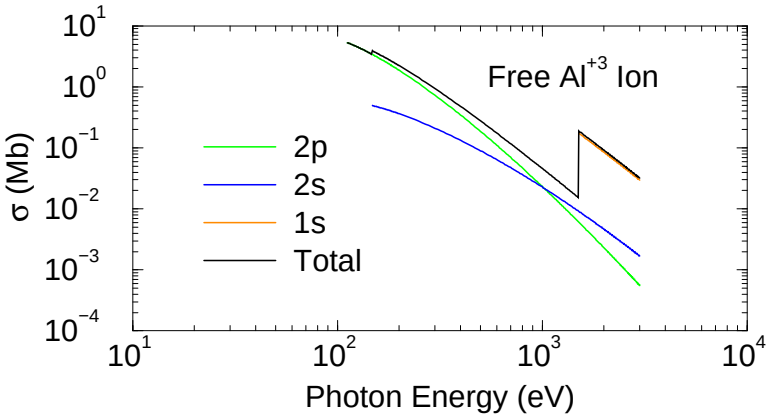

Figure 3: Photoionization cross section for an isolated Al^{+3} ion.

Rozsnyai. The differences between the present IPA values of oscillator strengths and the correlated values from the SCRPA calculation are unexpectedly small.

2.6 Applications: Photoionization

Aluminum As mentioned earlier, photoexcitation and photoionization of Al and Cs at low temperatures and densities was considered by Rozsnyai [20]. In the previous subsection, we gave our values for the oscillator strengths of discrete transitions in an Al plasma with density 0.027 gm/cc at temperature kT=10 eV. Here we continue that discussion by considering photoionization of an average atom in the same plasma. The energies and occupation numbers of an average atom in this plasma were shown previously in Table 2. As noted earlier, the Ne-like core subshells are almost completely occupied and the remaining bound levels are sparsely occupied. The cross section for photoionization of the core subshells is therefore expected to be similar to that for a free Al^{+3} ion, which is shown in Fig. 3. This cross section was obtained using the Hartree-like model potential given in Ref. [23]. The contribution to the cross section from each of the three subshells is shown in the figure.

The corresponding result for our average atom is shown in Fig. 4. Except for the rapid oscillations in the inner shell cross sections near threshold, the inner-shell cross sections are almost indistinguishable from the corresponding results for the Al^{+3} ion shown in Fig. 3. These oscillations are shown in much greater detail in Fig. 5. The radius of the Wigner-Seitz sphere in this case is R=13.879 a_0, and the resonances occur at those momenta for which an integral number of wave lengths of the continuum electron fit inside the Wigner-Seitz sphere.[4] The maxima in the cross section occur when anti-nodes of the contin-

[4] A similar phenomenon occurs in classical scattering of electromagnetic radiation from a dielec-

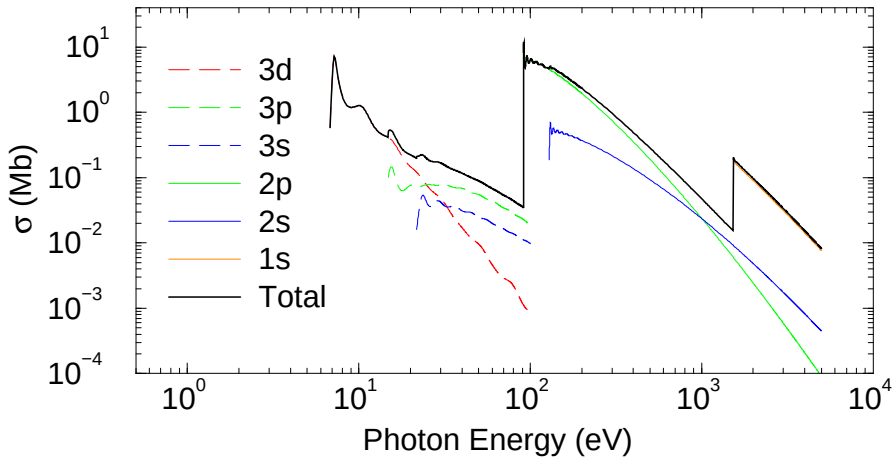

Figure 4: Photoionization cross section for an average atom in an Al plasma at density ρ_m=0.027 gm/cc and temperature kT=10eV.

uum wave function are at the boundary $r = R$ and minima occur when nodes are at $r = R$. The contributions to the cross section for energies below the $n = 2$ threshold near 100 eV arise entirely from the partially occupied levels with principal quantum numbers $n > 2$. The contributions from $n = 3$ subshells are shown in Fig. 4. The cross section found here is in fair agreement with that given Rozsnyai in Fig. 3 of Ref. [20].

In a coupled theory, such as the TDLDA, the strong dipole transitions from the $n = 2$ shells, shown in Table 3, lead to resonances in the $n = 3$ photoionization cross section. Thus, we expect resonances near $\omega = 70$ eV from the $2p \rightarrow 3s$ transitions, and resonances near 85 eV from $2p \rightarrow 3d$ transitions. Moreover, $2s \rightarrow 3p$ resonances are expected in the inner shell $2p$ cross section near 114 eV. Such resonances will dramatically alter the appearance of the cross section shown in Fig. 3. The influence of intershell coupling on photoabsorption was previously studied for an iron plasma at metallic density and kT=100 eV by Grimaldi *et al.* in Ref. [1] using nonrelativistic TDLDA .

tric sphere when the radius of the sphere is large compared to the wave length. A detailed analysis of this limiting case, referred to as van de Hulst scattering can be found in Ref. [24].

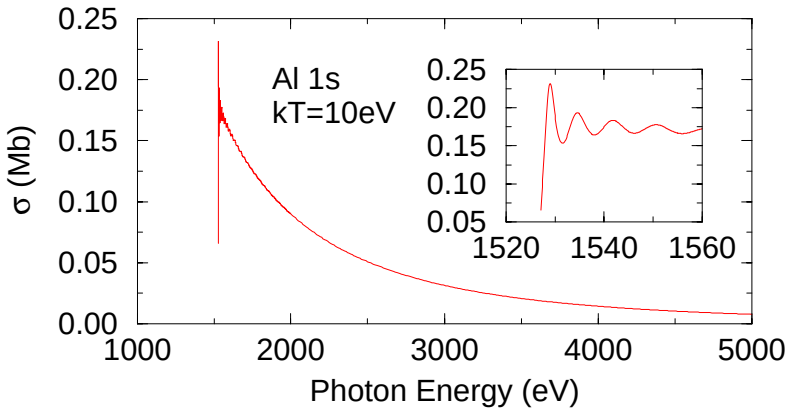

Figure 5: Photoionization cross section for the $1s$ subshell of average atom in an Al plasma at density ρ_m=0.027 gm/cc and temperature kT=10 eV. Resonances occur at momenta for which an integral number of photoelectron wavelengths are inside the Wigner-Seitz sphere.

Appendices

A Thomas-Fermi Electron Density

We consider an atom with N electrons moving in a potential $U(r)$. We suppose that locally the electrons are moving in a box of side L and depth $U(r)$. The number of states in momentum interval d^3p is

$$d^3N = 2\frac{L^3}{(2\pi)^3}d^3p \ ,$$

so that the particle density is

$$\rho = \frac{N}{L^3} = \frac{1}{\pi^2}\int_0^{p_f} p^2 dp = \frac{p_f^3}{3\pi^2} \ ,$$

at zero temperature, assuming levels up to the Fermi level p_f are occupied. At finite temperature T this generalizes to

$$\rho = \frac{1}{\pi^2}\int_0^{\infty} \frac{p^2 dp}{\left[1+e^{(E-\mu)/kT}\right]} \ ,$$

where E is the particle energy, μ is the chemical potential, and $k = 8.617342 \times 10^{-5}$ eV/K is Boltzman's constant. Taking advantage of the energy-momentum relation

$$\frac{p^2}{2m} + U(r) = E \ ,$$

we may change the independent variable to E. We have $pdp = mdE$, from which follows

$$\rho = \frac{m}{\pi^2} \int_{V(r)}^{\infty} \frac{pdE}{\left[1 + e^{(E-\mu)/kT}\right]} \ . \tag{A.1}$$

With the further change of variable $\epsilon = E - U$, $p = \sqrt{2m\epsilon}$, we obtain

$$\rho = \frac{(2m)^{3/2}}{2\pi^2} \int_{0}^{\infty} \frac{\sqrt{\epsilon}\, d\epsilon}{\left[1 + e^{(\epsilon+U(r)-\mu)/kT}\right]} \ . \tag{A.2}$$

It is convenient to write this expression in terms of the Fermi integral

$$I_{1/2}(x) = \int_{0}^{\infty} \frac{y^{1/2}\, dy}{\left[1 + e^{y-x}\right]} \ .$$

We find that

$$\rho(r) = \frac{(2mkT)^{3/2}}{2\pi^2}\, I_{1/2}(x)$$

with

$$x = \left[\mu - U(r)\right]/kT \, .$$

In our model, only those electrons with $E \geq 0$ are treated in the Thomas-Fermi approximation. With this understanding, Eqs. (A.1) and (A.2) become

$$\rho_c(r) = \frac{m}{\pi^2} \int_{0}^{\infty} \frac{pdE}{\left[1 + e^{(E-\mu)/kT}\right]} \tag{A.3}$$

$$= \frac{(2m)^{3/2}}{2\pi^2} \int_{-U(r)}^{\infty} \frac{\sqrt{\epsilon}\, d\epsilon}{\left[1 + e^{(\epsilon+U(r)-\mu)/kT}\right]}. \tag{A.4}$$

With the substitution $y = \epsilon/kT$, this becomes

$$\rho_c(r) = \frac{(2mkT)^{3/2}}{2\pi^2}\, I_{1/2}(b, x) \, , \tag{A.5}$$

where $I_j(b, x)$ is the incomplete Fermi-Dirac integral

$$I_j(b, x) = \int_{b}^{\infty} \frac{y^j\, dy}{1 + \exp[y - x]} \, , \tag{A.6}$$

with $b = U(r)/kT$. Equation (A.5), with $U(r) = V(r) - Z/r$, is used to evaluate the continuum contribution to the electron density in our model.

B Kohn-Sham Exchange Potential

The following is a reprise of the derivation of the Kohn-Sham exchange potential given in Ref. [25]. Let us consider an N electron atom and suppose that a given

state can be described by a single determinantal wave function $\Psi_{abc\cdots}$. The energy of the atom in this state can be written

$$E = \sum_a \langle a|h_0|a\rangle + \frac{1}{2}\sum_{ab}\iint \frac{d^3r_1 d^3r_2}{R}\phi_a^\dagger(r_1)\phi_a(r_1)\phi_b^\dagger(r_2)\phi_b(r_2)$$
$$-\frac{1}{2}\sum_{ab}\iint \frac{d^3r_1 d^3r_2}{R}\phi_a^\dagger(r_1)\phi_b(r_1)\phi_b^\dagger(r_2)\phi_a(r_2)\,. \qquad \text{(B.1)}$$

The term on the second line of Eq. (B.1) is the exchange energy $E_{\rm exc}$. The exchange energy is evaluated assuming that the single-particle orbitals are non-relativistic plane waves:

$$\phi_a(r) = \frac{1}{\sqrt{V}}e^{ip_a\cdot r}\chi_{\sigma_a}\,.$$

We find

$$E_{\rm exc} = -\frac{1}{2V^2}\sum_{\sigma_a\sigma_b}\left(\chi^\dagger_{\sigma_a}\chi_{\sigma_b}\right)\left(\chi^\dagger_{\sigma_b}\chi_{\sigma_a}\right)\sum_{p_a p_b}\iint\frac{d^3r_1 d^3r_2}{R}e^{iq\cdot R}\,, \qquad \text{(B.2)}$$

with $q = p_b - p_a$ and $R = r_1 - r_2$. We make use of the fact that

$$\frac{1}{V}\sum_{p_a} \to \frac{1}{(2\pi)^3}\int d^3p_a\,,$$

and

$$\sum_{\sigma_a\sigma_b}\left(\chi^\dagger_{\sigma_a}\chi_{\sigma_b}\right)\left(\chi^\dagger_{\sigma_b}\chi_{\sigma_a}\right) = \sum_{\sigma_a}\left(\chi^\dagger_{\sigma_a}\chi_{\sigma_a}\right) = 2\,,$$

to rewrite the expression for the exchange energy as

$$E_{\rm exc} = -\frac{1}{(2\pi)^6}\iint d^3r_1 d^3r_2\iint d^3p_a d^3p_b\frac{1}{R}e^{iq\cdot R}\,.$$

Change variables to $R = r_1 - r_2$, and $r = r_2$; then $d^3r_1 d^3r_2 = d^3R d^3r$ and the exchange energy becomes

$$E_{\rm exc} = -\frac{1}{(2\pi)^6}\int d^3r\iint d^3p_a d^3p_b\int\frac{d^3R}{R}e^{iq\cdot R}\,.$$

One can evaluate the innermost integral (with damping at large R) as

$$\int\frac{d^3R}{R}e^{iq\cdot R} = \frac{4\pi}{q^2}.$$

It follows that

$$E_{\rm exc} = -\frac{2}{(2\pi)^4}\int d^3r\int d^3p_a\int_0^{p_f}p_b^2 dp_b\int_{-1}^{1}\frac{d\mu}{p_a^2+p_b^2-2p_a p_b\mu}\,. \qquad \text{(B.3)}$$

The integral over μ can be carried out to give

$$\int_{-1}^{1} \frac{d\mu}{p_a^2 + p_b^2 - 2p_a p_b \mu} = \frac{1}{p_a p_b} \ln\left(\frac{p_a + p_b}{|p_a - p_b|}\right).$$

The integral over p_b is next carried out to give

$$\int_0^{p_f} dp_b \frac{p_b}{p_a} \ln\left(\frac{p_a + p_b}{|p_a - p_b|}\right) = \frac{1}{2p_a}\left[\left(p_f^2 - p_a^2\right) \ln\left(\frac{p_f + p_a}{p_f - p_a}\right) + 2p_f p_a\right].$$

The integral over d^3p_a is next carried out to give

$$2\pi \int_0^{p_f} dp_a\, p_a \left[\left(p_f^2 - p_a^2\right) \ln\left(\frac{p_f + p_a}{p_f - p_a}\right) + 2p_f p_a\right] = 2\pi p_f^4$$

This gives us finally,

$$E_{\rm exc} = -\frac{2}{(2\pi)^3} \int d^3r\, p_f^4 = -\frac{3}{4\pi}(3\pi^2)^{1/3} \int d^3r \rho^{4/3}(r)\,, \tag{B.4}$$

where we have used the relation

$$p_f = (3\pi^2 \rho(r))^{1/3}$$

to express the Fermi-momentum in terms of the particle density.

Variational Equations We may express the energy of a system of particles in terms of the electronic wave functions as

$$E = \int d^3r \left\{\sum_a \phi_a^\dagger h_0 \phi_a + \frac{1}{2}\int \frac{d^3r' \rho(r)\rho(r')}{R} - \frac{3}{4\pi}(3\pi^2)^{1/3}\rho^{4/3}(r)\right\}, \tag{B.5}$$

where

$$\rho(r) = \sum_a |\phi_a(r)|^2\,.$$

In our discussion, we require

$$N_a = \int d^3r |\phi_a(r)|^2 = 1\,.$$

The variation $\delta\phi_a^\dagger$ in the single-particle orbital ϕ_a leads to the variation

$$\begin{aligned}
&\delta\left[E - \epsilon_a N_a\right] \\
&\quad = \int d^3r\, \delta\phi_a^\dagger \left\{h_0\phi_a + \int \frac{d^3r'\,\rho(r')}{R}\phi_a - \left[\frac{3}{\pi}\rho(r)\right]^{1/3}\phi_a - \epsilon_a\phi_a\right\},
\end{aligned}$$

in $E - \epsilon_a N_a$, where ϵ_a is a Lagrange multiplier introduced to insure that the normalization constraint is satisfied. The condition $\delta\left[E - \epsilon_a N_a\right] = 0$ leads to the Kohn-Sham equations

$$\left(h_0 + \int \frac{d^3r'\,\rho(r')}{R} + V_{\rm exc}(r)\right)\phi_a = \epsilon_a \phi_a\,, \tag{B.6}$$

where

$$V_{\rm exc}(r) = -\left[\frac{3}{\pi}\rho(r)\right]^{1/3}\,. \tag{B.7}$$

As shown in [25], the Kohn-Sham exchange potential is related to the average exchange potential introduced earlier by Slater [26] by

$$V_{\rm exc}(r) = \frac{2}{3}\,V_{\rm Slater}(r)\,.$$

Practical Matters In numerical codes, one deals with the radial parts $P_a(r)$ of the orbitals $\phi_a(r)$,

$$\phi_a(r) \equiv \phi_{n_a l_a m_a \sigma_a}(r) = \frac{1}{r} P_{n_a l_a}(r) Y_{l_a m_a}(\hat{r}) \chi_{\sigma_a}\,,$$

which are normalized by

$$\int_0^\infty dr\ \left[P_{n_a l_a}(r)\right]^2 = 1\,.$$

The corresponding radial density for the atom is

$$n(r) = \sum_a g_a P_a^2(r)\,,$$

where g_a is the occupation number of the subshell $a \equiv (n_a l_a)$. Averaging over angles, one obtains

$$\int_0^\infty dr\, n(r) = N\,,$$

where N is the total number of electrons in the atom. We write the density in terms of the radial density as

$$\rho(r) = \frac{1}{4\pi r^2} n(r)\,,$$

and consequently

$$V_{\rm exc}(r) = -\left[\frac{3}{4\pi^2}\frac{n(r)}{r^2}\right]^{1/3}\,. \tag{B.8}$$

C MIT Bag Model

The Thomas-Fermi model automatically confines the continuum density $\rho_c(r)$ to the region inside the Wigner-Seitz sphere, $r \leq R$. We also wish to constrain the bound-state density $\rho_b(r)$ to lie within the sphere. Nonrelativistically, this can be done by introducing a very high potential barrier outside the sphere. As the barrier height increases, the bound-state radial wave functions $P_{nl}(r)$ gets smaller and smaller at $r = R$, and, in the limit of an infinite potential, $P_{nl}(R) \to 0$.

The well-known Klein paradox [27] shows us that a relativistic particle can *not* be similarly confined by an arbitrarily high potential barrier. Nevertheless, confinement of a relativistic particle to a sphere of radius R can be achieved, using the MIT bag-model [28] boundary condition $P_{n\kappa}(r) = Q_{n\kappa}(R)$. This condition, as shown below, is obtained by letting the particle's mass m increase to a large value in the region $r > R$.

The radial Dirac equations in the field-free region beyond the Wigner-Seitz cavity may be written.

$$c\frac{dQ}{dr} = (E - mc^2)P \,, \tag{C.1}$$

$$c\frac{dP}{dr} = -(E + mc^2)Q \,. \tag{C.2}$$

This pair leads to the second-order equation

$$c^2\frac{d^2P}{dr^2} + (E^2 - m^2c^4)P = 0 \,,$$

which has two linearly independent solutions $e^{\pm\lambda r}$, with $\lambda = \sqrt{m^2c^2 - E^2/c^2}$. The corresponding solutions are

$$P^{\pm}(r) = \sqrt{\frac{mc^2 + E}{2mc^2}}\; e^{\pm\lambda r}$$

$$Q^{\pm}(r) = \mp\sqrt{\frac{mc^2 + E}{2mc^2}}\; e^{\pm\lambda r}$$

Now, if we replace $m \to M \gg m$, but fix the energy E, then the radial functions associated with the solution that is regular at infinity becomes

$$P^{-}(r) \to \sqrt{\frac{1}{2}}\; e^{-Mcr}$$

$$Q^{-}(r) \to \sqrt{\frac{1}{2}}\; e^{-Mcr} \,.$$

It follows from these relations that to match a solution to the Dirac equation inside the sphere to a large-mass solution beyond the sphere, we must have $P(R) = Q(R)$ at the boundary. It should be emphasized that the density does

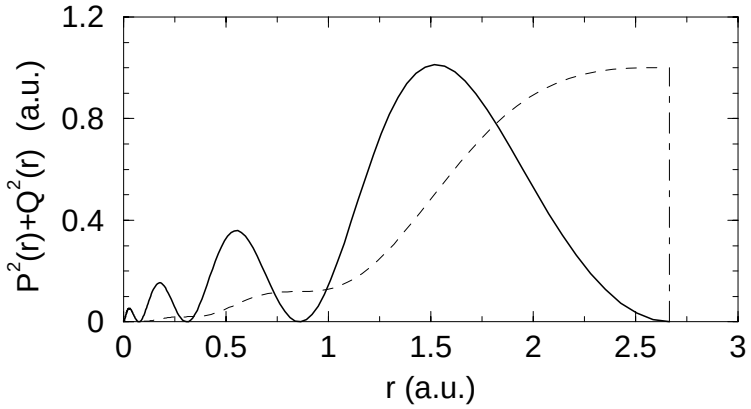

Figure 6: The radial density of an average-atom $4s$ electron in an iron plasma of normal density and temperature kT=100 eV is shown in the solid line and the integrated probability density is shown in the dashed line. The $4s$ radial wave functions satisfy the MIT bag-model boundary conditions on the surface of the Wigner-Seitz sphere.

not vanish at $r = R$, it simply approaches a finite (but small) value on the boundary. The finite wave functions inside connect to functions that vanishes exponentially outside the cavity. As M approaches infinity, the fall-off distance drops to zero!. In Fig. 6, we show the radial density of a $4s$ electron that satisfies the bag-model boundary conditions. This wave function is from the iron plasma considered in the example of Section 1.2.

The practical problem that we face is how to set up $P(r)$ and $Q(r)$ at a few points beyond $r = R$ in such a way that the bag-model boundary conditions are satisfied at $r = R$ and that $P(r)$ and $Q(r)$ are solutions of the equation with mass m. Such initial values are needed to obtained "ingoing" solutions to the radial Dirac equation. A combination of the mass m solutions which reduces to $P(R) = Q(R)$ is

$$\begin{aligned} P(r) &= e^{\lambda r} + a\, e^{\lambda(2R-r)} \\ Q(r) &= \frac{c\lambda}{c^2+E}\left[-e^{\lambda r} + a\, e^{\lambda(2R-r)}\right] . \end{aligned}$$

where

$$a = -\frac{(c\lambda + c^2 + E)^2}{2E(c^2+E)} = -\frac{(2 + \lambda/c + W/c^2)^2}{2(1+W/c^2)(2+W/c^2)} .$$

For numerical stability the second form is probably better. It is also useful to use the alternative expression for λ:

$$\lambda = \sqrt{-W(2+W/c^2)} .$$

In both expressions, $W = E - c^2$.

References

[1] F. Grimaldi, A. Grimaldi-Lecourt, and M. W. C. Dharma-wardana, Phys. Rev. A **32**, 1063 (1985).

[2] D. A. Liberman, J. Quant. Spectrosc. Radiat. Transfer **27**, 35 (1982); B. I. Bennett and D. A. Liberman, Los Alamos National Laboratory Report No. LA-10309-M (1985).

[3] R. P. Feynman, N. Metropolis, and E. Teller, Phys. Rev. **75**, 1561 (1949).

[4] R. D. Cowan and J. Ashkin, Phys. Rev. **105**, 144 (1957).

[5] B. F. Rozsnyai, Phys. Rev. A**5**, 1137 (1972).

[6] T. Belenski and K. Ishikawa, Phys. Rev. E**51**, 4869 (1995).

[7] URL: http://www.webelements.com/webelements/

[8] A. Zangwill and P. Soven, Phys. Rev. A**21**, 1561 (1980); Phys. Rev. Lett. **45**, 204 (1980).

[9] F. A. Parpia, Ph. D. Thesis, Notre Dame University, 1984, (unpublished).

[10] F. A. Parpia and W. R. Johnson, J. Phys. B**16**, L375 (1983); B**17** 531 (1984).

[11] F. A. Parpia, W. R. Johnson, and V. Radojevic, Phys. Rev. A**29**, 3173 (1984).

[12] F. A. Parpia and W. R. Johnson, Phys. Lett. A**99**, 172 (1983).

[13] W. R. Johnson, in *Advances in Atomic and Molecular Physics*, eds. D. Bates and B. Bederson, v. 25, p. 375 (Academic Press, San Diego, 1988).

[14] J. des Cloizeaux, in *Many-Body Physics*, eds. C. de Witt and R. Balian, p. 5 (Gordon and Breach,New York,1968).

[15] G. Csanak and D. P. Kilcrease, J. Quant. Spectrosc. Radiat. Transfer **58** 537 (1997).

[16] G. Csanak and G. D. Meneses, LANL Internal Report, LA-UR-00-5597 (2000).

[17] M. Ya. Amusia and N. A. Cherepkov, Case Studies in Atomic Physics, **5**, 47 (1975).

[18] C. M. Lee and W. R. Johnson, Phys. Rev. A**22**, 979 (1980).

[19] W. R. Johnson, K. T. Cheng, K.-N. Huang, and M. LeDourneuf, Phys. Rev. A**22**, 989 (1980).

[20] B. F. Rozsnyai, J. Quant. Spectrosc. Radiat. Transfer **13** 1285 (1973).

[21] U. I. Safronova, private communication.

[22] B. F. Rozsnyai, J. Quant. Spectrosc. Radiat. Transfer **15** 695 (1975).

[23] A. Derevianko, W. R. Johnson, and K. T. Cheng, At. Data and Nucl. Data Tables **73**, 153 (1999).

[24] R. G. Newton, *Scattering Theory of Waves and Particles*, p. 65 (McGraw-Hill, New York, 1966).

[25] W. Kohn and L. J. Sham, Phys. Rev. **140**, A1133 (1965).

[26] J. C. Slater, Phys. Rev. **81**, 385 (1951).

[27] J. J. Sakurai, *Advanced Quantum Mechanics*, p. 120 (Addison-Wesley, Reading MA, 1967).

[28] A. Chodos, R. L. Jaffee, K. Johnson, C. B. Thorn, and V. W. Weisskopf, Phys. Rev. D**9**, 3471 (1974).